

Nitric Oxide Nanosensors for Predicting the Development of Osteoarthritis in Rat Model

Pan Jin,^{†,‡,§,#} Christian Wiraja,^{§,#} Jinmin Zhao,^{†,‡,§,#} Jinlu Zhang,^{†,‡,§} Li Zheng,^{*,†,‡,§} and Chenjie Xu^{*,‡,§,#}

[†]Guangxi Engineering Center in Biomedical Materials for Tissue and Organ Regeneration, [‡]Guangxi Collaborative Innovation Center for Biomedicine, and [§]Guangxi Key Laboratory of Regenerative Medicine, The First Affiliated Hospital of Guangxi Medical University, Nanning 530021, People's Republic of China

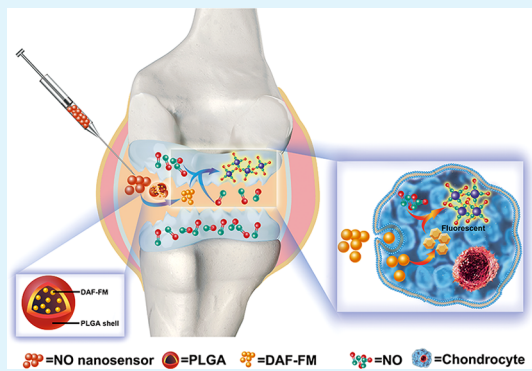
[#]School of Chemical and Biomedical Engineering, Nanyang Technological University, 70 Nanyang Drive, 637457 Singapore

^{*}NTU-Northwestern Institute for Nanomedicine, Nanyang Technological University, 50 Nanyang Avenue, 639798 Singapore

Supporting Information

ABSTRACT: Osteoarthritis (OA) is a chronic arthritic disease that causes the overproduction of inflammatory factors such as nitric oxide (NO). This study develops a NO nanosensor to predict the OA development. The nanosensor is synthesized by encapsulating the NO sensing molecules (i.e., 4-amino-5-methylamino-2',7'-difluorofluorescein Diaminofluorescein-FM (DAF-FM)) within the biodegradable poly(lactic-co-glycolic acid) nanoparticles. In vitro, the nanosensor allows the monitoring of the NO release in interleukin-1 β -stimulated chondrocytes and the alleviated effect of N^G-monomethyl-L-arginine (a NO inhibitor) and andrographolide (an anti-inflammatory agent). In the rat OA model, it permits the quantification of NO level in joint fluid. The proposed NO nanosensor may facilitate a noninvasive and real-time evaluation of the OA development.

KEYWORDS: nanosensor, nitric oxide sensing, osteoarthritis, DAF-FM, PLGA



1. INTRODUCTION

Osteoarthritis (OA) is a chronic condition with a significant disease burden, affecting 15% of the population worldwide.^{1,2} A key molecule in the inflammatory and degradative cascade of arthritis, nitric oxide (NO) is noted as a potential biomarker of the inflammation in OA.³ Its overproduction is the result of the overexpression of an inducible nitric oxide synthase (iNOS or NOS2) caused by the stimuli of proinflammatory cytokines, such as tumor necrosis factor α and interleukin-1 β (IL-1 β). Studies have shown that NO increases the expression of active matrix metalloproteinases (MMPs), inhibits the matrix protein synthesis, modulates prostaglandin E2 (PGE2) synthesis, and, under some conditions, may initiate chondrocyte apoptosis.^{3,6} NO is present in the plasma of OA patients and more prominently in the synovial fluid.^{7,8}

The in vitro NO secretion is often measured via fluorescence microscopy using diaminofluorescein-based probes (e.g., 4-amino-5-methylamino-2',7'-difluorofluorescein Diaminofluorescein-FM, DAF-FM).⁹ The aromatic vicinal diamines of diaminofluorescein can react with NO in the presence of O₂ to form the corresponding triazole compounds, resulting in a turn-on emission because the quenching extent of the triazole groups is smaller than that of the electron-rich amino groups.¹⁰ These fluorescent sensors are quite sensitive to NO with a detection limit in the nanomolar range. Their cell permeability can be

improved by converting the probe (e.g., DAF-FM) to a diacetateform (e.g., DAF-FM diacetate). Despite their sensitivity to NO and the convenience in usage, these molecular sensors also come with several disadvantages.¹¹ First, they react with other biological molecules such as dehydroascorbic acid and ascorbic acid, thus contributing to false signals. Second, the pH condition may also affect the fluorescence intensity.¹² Finally, as small molecules, these probes are poorly retained within the cells or tissue and are quickly excreted or secreted. Thus, there has not been any progress to track the NO production in OA animal model. Although efforts are being spent on developing new molecular sensors or setting independent verification using spectroscopic or electrochemical methods,¹³ an alternative solution is needed to allow continual usage of these sensitive molecular sensors to track NO in the OA model.

Previously, we explored the utilization of nanoparticle encapsulation to extend the cellular retention of molecular beacons or viability-sensing molecules in stem cell tracking.^{14,15} Inspired by those works, we hypothesize that nanoparticle encapsulation could address the above-mentioned challenges of

Received: May 7, 2017

Accepted: July 10, 2017

Published: July 10, 2017

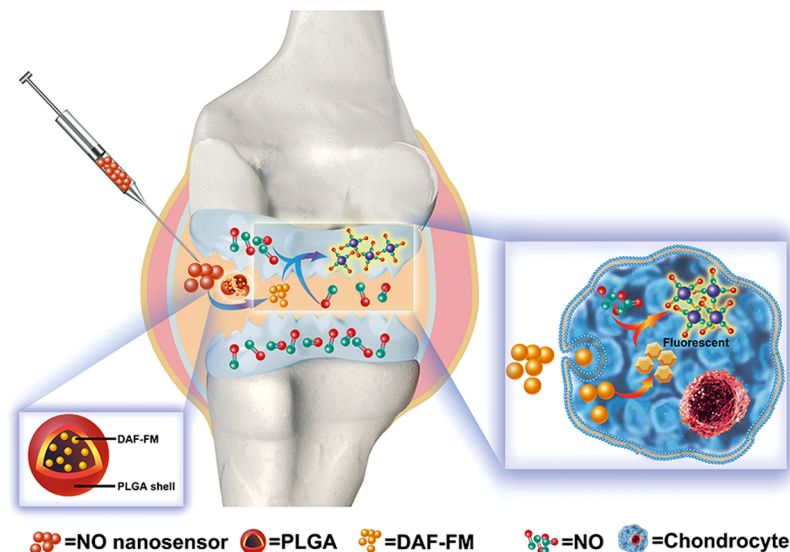


Figure 1. Schematic illustration of NO nanosensors application for predicting OA development.

diaminofluorescein-based molecular probes. As a proof of concept, we synthesize a NO nanosensor by encapsulating the DAF-FM within poly(lactic-co-glycolic acid) (PLGA) nanoparticles (Figure 1) for predicting the OA progression.

2. MATERIALS AND METHODS

2.1. Synthesis and Characterization of NO Nanosensor. NO nanosensor (DAF-FM-containing PLGA nanoparticle) was synthesized using the single emulsion method. Briefly, 500 μg DAF-FM (D1821; Sigma-Aldrich, Saint Louis, MO) was mixed with 50 mg PLGA (50:50, molecular weight of 10 kDa) in 2 mL chloroform at 4 °C. Subsequently, the mixture was added dropwise to 3% poly(vinyl alcohol) solution and homogenized (Tissue Master 125; Omni International) for 60 s at 24 000 rpm. Then, the emulsion was placed in a chemical hood for 4 h to evaporate chloroform. Finally, the nanosensors were centrifuged at 10 000 rpm and rinsed thrice with distilled water prior to freeze-drying. The hydrodynamic diameter and the zeta potential of the nanosensors were quantified using Zetasizer Nano Z (Malvern Instruments Ltd, U.K.). Their morphology was examined with JSM-6700F field-emission scanning electron microscope (JEOL USA, Inc.).

The release profile of DAF-FM was studied in a cell culture medium at 37 °C. Absorbance of the supernatants at 495 nm was obtained at the designated time points (i.e., 0, 6, 12, 24, 48, 72, 96, and 144 h) using a UV-2450 ultraviolet-visible (UV-vis) spectrophotometer (Shimadzu Corporation, Kyoto, Japan). The DAF-FM in the supernatants was quantified by fitting the concentration–absorbance standard curve of DAF-FM and then normalizing it against the original loaded quantity.

The stability of DAF-FM probe inside the nanosensor was similarly evaluated by measuring the fluorescence intensity of the nanosensor release supernatant (495/515 nm) against DAF-FM solution incubated for the same period at 37 °C.

2.2. Articular Chondrocytes Isolation and Culture. Primary articular chondrocytes were isolated from the knee joints of the neonatal Sprague–Dawley (SD) rats (3–7 days old, Animal Resources Centre of Guangxi Medical University, Nanning, Guangxi, China) through collagenase digestion as described previously.¹⁶ Briefly, cartilage was separated from the joints, sectioned into pieces, dissociated with 2 mg/mL collagenase type II (Gibco), and cultured in α -modified Eagle's medium (Gibco) containing 10% (v/v) fetal bovine serum (Gibco) and 1% (v/v) penicillin/streptomycin (Solarbio). Chondrocytes at passage 2 were used for further studies.

2.3. Cytotoxicity Assay. Cytotoxicity was examined with the cell-counting Kit-8 (CCK-8; Dojindo Laboratories, Kumamoto, Japan).

Briefly, the chondrocytes were treated with IL-1 β , andrographolide (abbreviation: Andro), and N^G-monomethyl-L-arginine (L-NMMA) and then added with CCK-8 reagent at 37 °C for 4 h. The absorbance at 450 nm was measured using a microplate reader (Thermo Scientific Multiskan GO Microplate Spectrophotometer) and the cell numbers were calculated with a calibration curve.

2.4. IL-1 β -Induced Chondrocytes and Treatment. Cells were divided into four groups: normal control (untreated chondrocytes), IL-1 β group (chondrocytes treated with 10 ng/mL IL-1 β), IL-1 β + L-NMMA group (chondrocytes cultured with 10 ng/mL IL-1 β along with L-NMMA (an iNOS inhibitor) of recommended concentration), and IL-1 β + Andro group (chondrocytes incubated with 10 ng/mL IL-1 β and Andro (an anti-inflammatory drug) of optimal dose). Cells were cultured for 2, 4, and 6 days, respectively. IL-1 β was acquired from PeproTech (New Jersey). L-NMMA (monoacetate salt) was purchased from Beyotime Institute of Biotechnology, Jiangsu, China. Andro (Chengdu Must Bio-technology Co. Ltd, Sichuan, China) was prepared in dimethyl sulfoxide (DMSO) with the final concentration of 100 mM. The final concentration of DMSO was less than 0.1%.

2.5. Fluorescence Intensity Analysis with NO Nanosensors. After 2, 4, and 6 days of culture, respectively, 1 mg/mL NO nanosensors were added in the culture medium in all of the groups. After 6 h of incubation at 37 °C, the supernatants were collected and the fluorescence intensity was recorded with a fluorescence microplate reader (Synergy H1; Bio-Tek Instruments, Inc.) at 495/515 nm.

2.6. NO Quantification in the Cell Supernatant. At days 2, 4, and 6, the cell supernatants in all of the groups were collected for detection of NO levels using a NO detection kit (Nanjing Jiancheng Biotechnology Research Institute, China) according to the manufacturer's protocol.

2.7. Cell Labeling and Imaging with NO Nanosensors. For imaging purposes, the cells were labeled with nanosensor and DAF fluorescence was captured. First, the cells were treated with 1 mg/mL nanosensor or DAF-FM. Subsequently, the cells were washed with phosphate-buffered saline, incubated in a dark environment with 70 nM rhodamine-phalloidin (Cytoskeleton, Inc.) for 30 min, and then stained with 1 $\mu\text{g}/\text{mL}$ Hoechst 33258 (Sigma) for 5 min. The images were obtained by a laser scanning confocal microscope (Nikon A1).

2.8. Gene Analysis with Quantitative Real-Time Polymerase Chain Reaction (RT-PCR). RNA was extracted from the cells using an RNA extraction kit (Tiangen Biotech Co., Ltd., China). The RNA was reverse transcribed using a reverse transcription kit (Fermentas Company). The RT-PCR reaction was carried out using a quantitative PCR detection system (Realplex 4; Eppendorf Corporation) with FastStart Universal SYBR Green Master (Roche). The PCR primers for the OA-related genes are presented in Table 1. Gene expression

Table 1. Primers for RT-PCR^a

| gene name | forward primer | reverse primer |
|----------------|-----------------------------|-----------------------------|
| β -actin | 5'-CCCATCTATGAGGGTACGC-3' | 5'-TTTAATGTCACGCACGATTTC-3' |
| Nos2 | 5'-GCTTGGGTCTTGTAGCCTAGT-3' | 5'-ATTCTGTGCAGTCCCAGTGAG-3' |
| Il1b | 5'-GCACAGTCCCCAACTGGTA-3' | 5'-GGAGACTGCCATTCTCGAC-3' |
| Mmp13 | 5'-GGATCCATGATGGCACTGCT-3' | 5'-TGGCTTTGCCAGTGTAGGT-3' |
| Ptgs2 | 5'-GATGACGAGCGACTGTTCCA-3' | 5'-CAATGTTGAAGGTGTCCGGC-3' |
| Col2a1 | 5'-GTCCTACAATGTCAGGGCCA-3' | 5'-ACCCCTCTCCCTGTAC-3' |
| Acan | 5'-GACAAGGACGAGTCCCTGG-3' | 5'-CTCCGGGATGTGGCATAAA-3' |

^a β -actin, β -actin as the normalization control; Nos2, nitric oxide synthase 2; Il1b, interleukin-1 β ; Mmp13, matrix metallopeptidase 13; Ptgs2, prostaglandin-endoperoxide synthase 2; Col2a1, collagen type II α 1 chain; Acan, aggrecan.

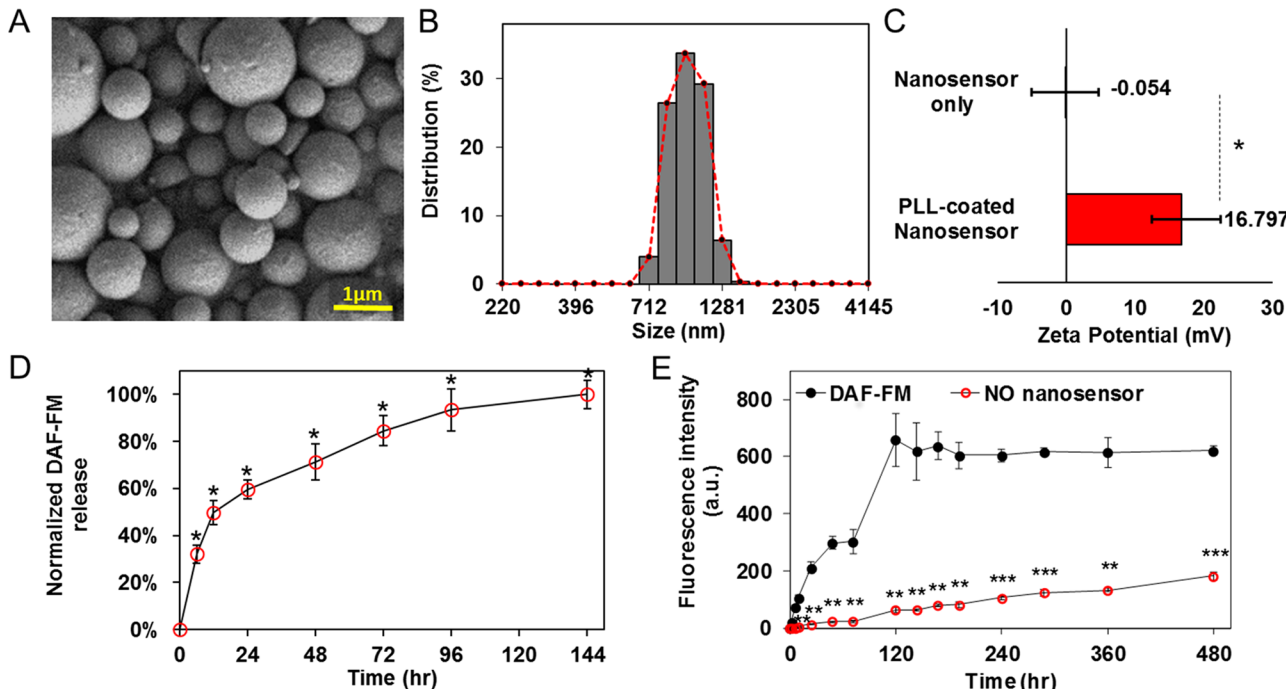


Figure 2. Synthesis and characterization of NO nanosensors. (A) Scanning electron microscope imaging of nanosensors (scale bar = 1 μ m). (B) Hydrodynamic diameter characterization of NO nanosensors. (C) Zeta potential of NO nanosensors (* indicates $p < 0.05$ compared with uncoated nanosensors, $N = 4$). (D) DAF-FM release from nanosensors (* indicates $p < 0.05$ compared with data at 0 h, $N = 4$). (E) Stability of NO nanosensors vs DAF-FM probe (** indicates $p < 0.01$ and *** indicates $p < 0.001$ for NO nanosensors vs DAF-FM probe at the same time point, $N = 4$). Data are presented as mean \pm standard deviation.

was analyzed using the $2^{-\Delta\Delta CT}$ method with β -actin as the control. Each sample was repeated in triplicate to reduce operation bar errors.

2.9. OA Induction in Rats and the Treatment. A total of 100 male SD rats weighing 210–240 g were used in the experiment. All of the animal experiments were performed in accordance with the ethical approval by the Institutional Ethics Committee of Guangxi Medical University (2015-03-21). After being anesthetized with 2% pentobarbital sodium solution via intraperitoneal injection, an anterior cruciate ligament transection (ACLT) was performed on the right hind limb of the rats to induce arthritis.¹⁷ The same incision was created on the left hind limb as the sham group. The animals were randomly divided into two groups: OA group and treatment group. In the OA group, the animals received an intra-articular injection of 0.3 mL normal saline after ACLT operation once per week for 4, 8, and 12 weeks. The treatment group was divided into two subgroups: one received an intra-articular injection of 1000 μ M L-NMMA and the other 50 μ M Andro once per week for 8 weeks after 4 weeks of ACLT operation.

2.10. In Vivo Imaging of NO Nanosensor-Labeled Joints. Animals were immobilized using 2% anesthetic isoflurane (2% in O₂). For in vivo imaging, the hair of the rat's hind limb was removed to reduce autofluorescence. Each rat was intra-articularly injected with 0.3 mL of 40 mg/mL NO nanosensors or fluorescent dye solution.

Throughout the whole experiment, the body temperature of the rat was kept constant with heating pads and rectal measurement of their body temperature. Fluorescence imaging was obtained at 0.5, 1, 2, and 3 h after the injection of the probe using the fluorescence imaging system (In-Vivo FX PRO; Bruker Corporation, Baden-Württemberg, Germany) at 495 nm excitation and 515 nm emission. Regions of interest were placed identically over both knees, within which the total fluorescence intensity was measured.

2.11. NO Quantification in Joint Synovial Fluid. The rats were sacrificed after the fluorescence imaging. Knee joint fluid was obtained through joint extract and stored at -20 °C before analysis. The NO concentration in the joint fluid was assessed by the NO detection kit (Nanjing Jiancheng Bioengineering Research Institute, China).

2.12. Macroscopic Observation of the Cartilage Damage in the Joints. The joints of all of the experiment animals were harvested for macroscopic observation and histological evaluation. Macroscopic evaluation was performed by two independent observers who were blinded to the treatment group. The depth of lesions of the articular cartilage was measured on a scale of 0–4 as described by Pelletier et al.¹⁸

2.13. Histological Analysis of the Cartilage Damage in the Joints. After macroscopic observation, the knee joints were immediately fixed in 4% paraformaldehyde and then decalcified with

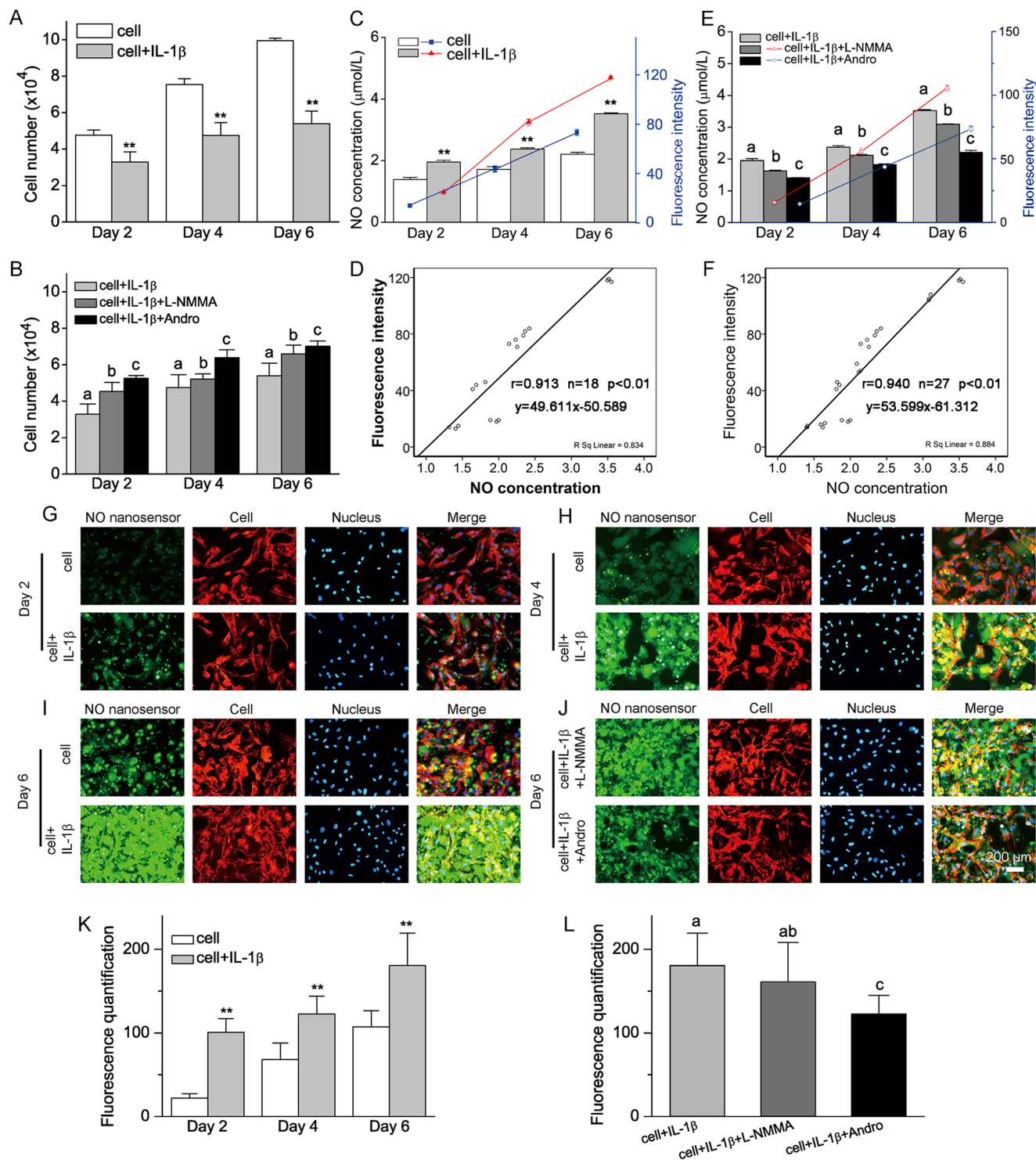


Figure 3. Tracking of the NO secretion in IL-1 β -stimulated chondrocytes with NO nanosensors. (A) The effect of IL-1 β on the proliferation of chondrocytes. (B) The effect of L-NMMA and Andro on the proliferation of IL-1 β -stimulated chondrocytes. (C) The effect of IL-1 β on the NO secretion of chondrocytes with corresponding nanosensor fluorescence (bars represent NO secretion, curve lines represent fluorescence intensity). (D) Correlation analysis of NO secretion and fluorescence intensity of chondrocytes and IL-1 β -stimulated chondrocytes in the measurement ($r = 0.913, n = 18, p < 0.01$). (E) The effect of L-NMMA and Andro on the NO secretion of IL-1 β -stimulated chondrocytes with the corresponding nanosensor fluorescence (bars represent NO secretion, curve lines represent fluorescence intensity). (F) Correlation analysis of fluorescence intensity of IL-1 β -stimulated chondrocytes treated with L-NMMA and Andro in the measurement against NO secretion ($r = 0.940, n = 27, p < 0.01$). (G–J) Fluorescence imaging of nanosensor-labeled chondrocytes in the IL-1 β treatment at day 2 (G), 4 (H), and 6 (I) (scale bar = 200 μm). (J) Fluorescence imaging of nanosensor-labeled chondrocytes treated with IL-1 β /L-NMMA and IL-1 β /Andro at day 6 (scale bar = 200 μm). (K) Fluorescence quantification of nanosensor-labeled chondrocytes at days 2, 4, and 6 after the IL-1 β treatment. (L) Fluorescence quantification of nanosensor-labeled chondrocytes treated with IL-1 β /L-NMMA and IL-1 β /Andro at day 6. Values are presented as mean \pm standard deviation; ** indicates $p < 0.01$, bars with different letters at the same time point are significantly different from each other at $p < 0.05$ and those with the same letter exhibit no significant difference.

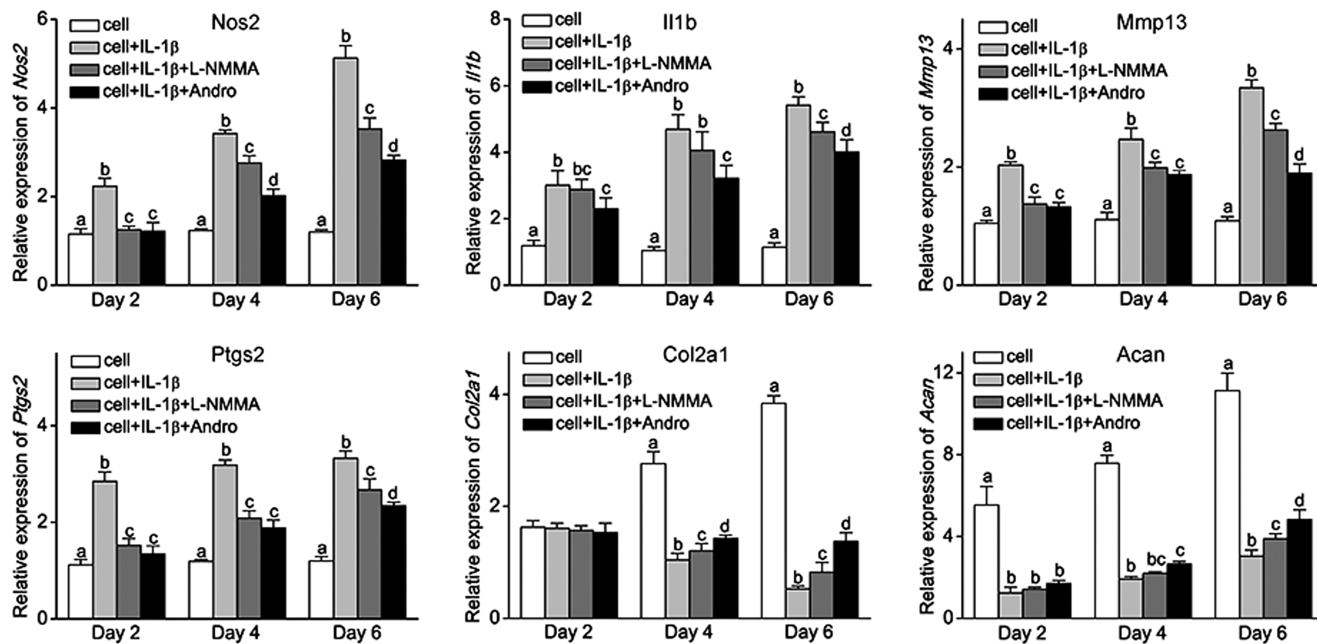


Figure 4. Relative mRNA levels of nitric oxide synthase 2 (*Nos2*), IL-1 β (*Il1b*), MMP13 (*Mmp13*), prostaglandin-endoperoxide synthase 2 (*Ptgs2*), COL2A1 (*Col2a1*), and aggrecan (*Acan*) on IL-1 β -stimulated chondrocytes and those treated with L-NMMA and Andro. Values are presented as mean \pm standard deviation; bars with different letters at the same time point are significantly different from each other at $p < 0.05$ and those with the same letter exhibit no significant difference.

buffered ethylenediaminetetraacetate. The samples were embedded in paraffin and serially sectioned from the medial compartment of the joints in the mid-sagittal plane. After dewaxing, 5 μ m thick sections were stained with hematoxylin and eosin (H&E) staining and Safranin-O-Fast green staining, respectively. Cartilage destruction was scored by two blinded observers using the histological grading system.¹⁹

2.14. Immunohistochemical Analysis. Immunohistochemical analysis was performed on the articular cartilage to investigate the protein expressions of collagen type II α 1 chain (COL2A1). Briefly, the sections were incubated with a primary antibody of COL2A1 (BA0533; Boster Biological Technology, Ltd., Wuhan, China, 1:100). After incubation with the second antibody and biotin-labeled horse radish peroxidase, the specimens were processed with a 3,3'-diaminobenzidine tetrahydrochloride kit (Boster) and counterstained with hematoxylin. The images were captured using an inverted phase contrast microscope (Olympus, Tokyo, Japan).

2.15. Western Blot Analysis. The cartilage tissues were scraped with a blade and pulverized in liquid nitrogen. Sixty micrograms of protein was extracted, loaded on a 10% (v/v) polyacrylamide gel, and transferred to poly(vinylidene difluoride) membrane (Millipore) using electroblotting. After being blocked with 5% nonfat dry milk, the specimens were incubated with a primary antibody of matrix metalloproteinase 13 (MMP13, ab75606, Abcam, 1:200), PTGS2 (cst12282; Cell Signaling Technology, Inc., 1:500), NOS2 (ab15323; Abcam, 1:40), and β -actin (ACTB, A2228, 1:1000), probed with an Alexa infrared dye-conjugated secondary antibodies (Invitrogen), and visualized using Odyssey Infrared Imaging System (LI-COR Biotechnology). The data were normalized against β -actin for each protein.

2.16. Correlation Analysis. Associations between NO concentration and fluorescence intensity were tested by calculating the Spearman correlation coefficients (r^2 ; very weak: 0–0.20, weak: 0.20–0.39, moderate: 0.40–0.59, strong: 0.60–0.79, very strong: 0.80–1).²⁰

2.17. Statistical Analysis. Student's *t*-test and ANOVA with posthoc tests were used for pairwise comparisons and multi-comparisons, respectively, after confirming a normal distribution using the Shapiro-Wilk test. SPSS software (version 16.0; SPSS Inc., Chicago, IL) was used and $p < 0.05$ was considered as significant difference.

3. RESULTS

3.1. NO Nanosensor Synthesis and Characterization.

NO nanosensors were synthesized by encapsulating DAF-FM into biodegradable PLGA nanoparticles by the single-emulsion method. The nanosensors were about 1 μ m in size (Figure 2A,B). They carried almost neutral charges (-0.05 mV), except when being coated with poly-L-lysine ($+16.8$ mV) to facilitate the cellular internalization (Figure 2C). Upon dispersion in the cell culture medium, the PLGA shells degraded over time due to hydrolysis. Consequently, the encapsulated DAF-FM molecules were continuously released over a period of \sim 144 h, with an initial burst release of \sim 50% by the first 12 h, followed by a slower release of the remaining 50% until 144 h (Figure 2D). Interestingly, the DAF-FM's stability to hydrolysis was significantly improved after nanoparticle encapsulation (Figure 2E). In comparison, when an equivalent amount of DAF-FM was dissolved in a culture medium that showed complete degradation to DAF by day 5 (120 h), the rise in the fluorescence intensity of nanosensor-containing supernatant was significantly slower ($p < 0.01$ or 0.001), even after an extended period of 480 h.

3.2. IL-1 β Inhibits Chondrocyte Proliferation, Whereas L-NMMA/Andro Attenuates This Inhibition Effect. The proliferation of the chondrocytes under the presence of 10 ng/mL IL-1 β was 31.3, 36, and 45.5% less than that of the cells without IL-1 β treatment at each time point (Figure 3A). As iNOS inhibitors,²¹ both L-NMMA and Andro attenuated this inhibition (Figure S1 in Supporting Information). Compared with IL-1 β -treated chondrocytes, L-NMMA showed an increased proliferation of 36.4, 8.3, and 22.2%, whereas Andro enhanced it by 60.6, 33.3, and 29.6% on days 2, 4, and 6, respectively (Figure 3B).

3.3. Tracking of NO Secretion by IL-1 β -Stimulated Chondrocytes with NO Nanosensors. NO secretion was assessed by the NO detection kit and the fluorescence intensity

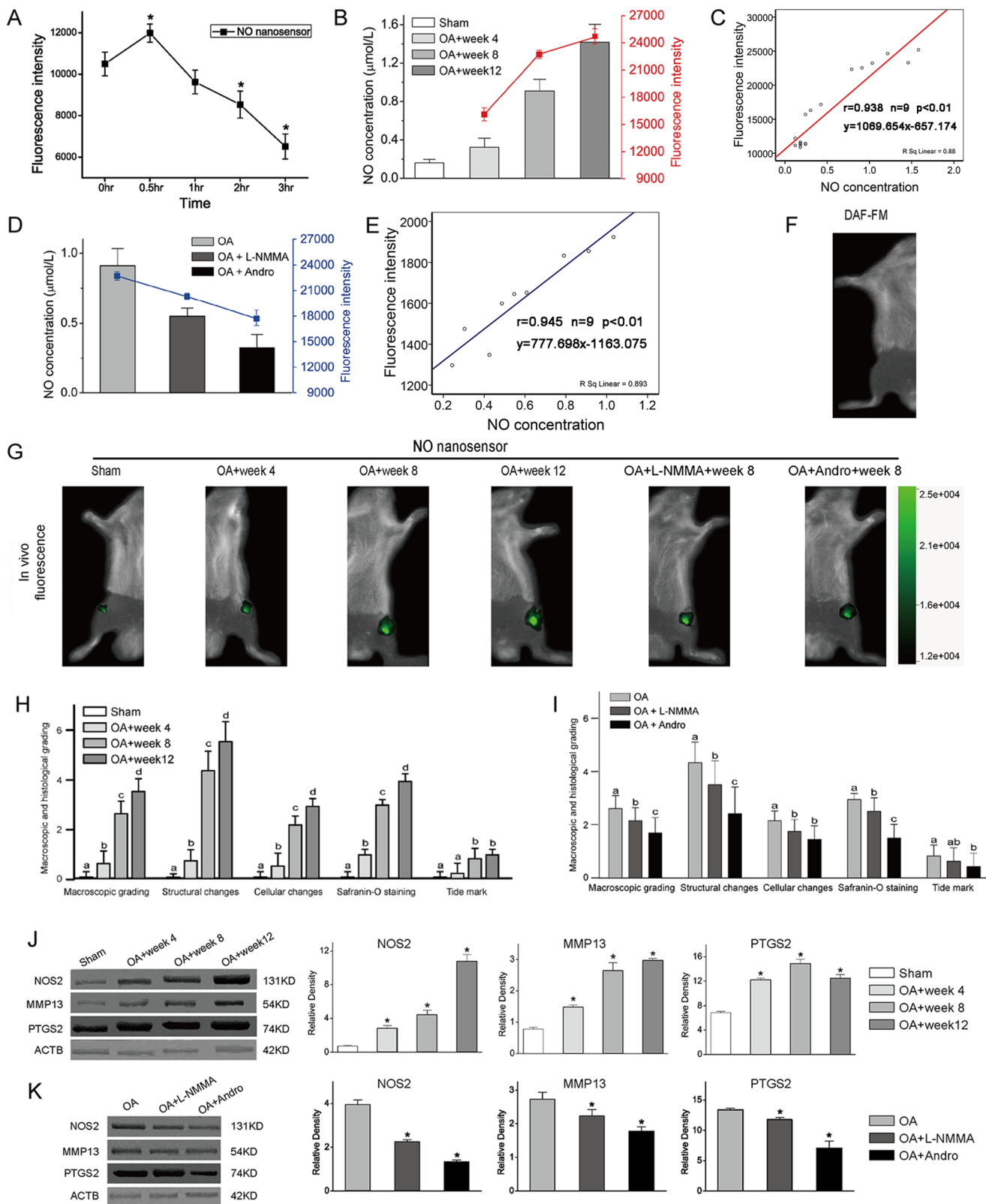


Figure 5. Tracking the NO secretion in the joints of OA animals with NO nanosensors. (A) Quantification of fluorescence from the normal rat joint after the intra-articular injection of NO nanosensors. (B) Quantification of the NO concentration in the synovial fluid from the OA knee joint with the NO detection kit, and nanosensor fluorescence intensity from the OA knee joints during the OA development. (C) Correlation analysis of the derived NO concentration and nanosensor fluorescence in the OA development. (D) The effect of L-NMMA and Andro on the NO secretion in synovial fluid and the nanosensor fluorescence of knee joints in the OA model at week 8. (E) Correlation analysis of the NO concentration and nanosensor fluorescence of the knee joints in the OA model treated with L-NMMA and Andro. (F) Fluorescence images of the normal joint of rats after the intra-articular injection of NO nanosensors. (G) Fluorescence detection of the OA-induced arthritis and that treated with L-NMMA and Andro. (H, I) Macroscopic and histological grading on the articular cartilage lesions of the OA-induced arthritis (H) and that treated with L-NMMA and Andro (I). (J, K) Western blot and densitometry for NOS2, MMP13, PTGS2, and ACTB in Sham, OA+week 4, OA+week 8, OA+week12 (J) and OA, OA+L-NMMA, OA+Andro (K) groups.

Figure 5. continued

and Andro (I). (J, K) Protein levels of NOS2, MMP13, and PTGS2 on the OA-induced arthritis (J) and that treated with L-NMMA and Andro (K). Values are presented as mean \pm standard deviation; * indicates $p < 0.05$, bars with different letters at the same time point are significantly different from each other at $p < 0.05$.

was determined by fluorescence microplate reader. As shown in Figure 3C, the chondrocytes treated with IL-1 β or untreated cells showed a time-dependent increase in fluorescence, which correlates with an increase in the NO levels. The fluorescence intensity of the chondrocytes treated or untreated with IL-1 β showed a positive correlation with NO secretion, with the correlation coefficient of 0.814 and 0.783, respectively (Figure 3D). The chondrocytes exposed to IL-1 β showed higher fluorescence and NO levels compared with untreated cells. In the treatment groups, both L-NMMA and Andro significantly downregulated the IL-1 β -increased NO production (Figure 3E). In these groups, the NO secretion was also highly correlated with the fluorescence intensity, with the correlation coefficients of 0.986 for Andro and 0.982 for L-NMMA treatment (Figure 3F).

For cell labeling, the chondrocytes treated with NO nanosensors were observed accompanied with phalloidin staining of the actin cytoskeleton (red) and cell nuclei (blue). As shown in Figure 3G–I, the cells proliferated over time in the both IL-1 β and untreated groups. As indicated by green fluorescence, the NO sensors mostly deposited on the cell membrane and overlapped most regions of the actin cytoskeletons. IL-1 β stimulated higher fluorescence compared with untreated cells. In IL-1 β groups, the fluorescence intensity increased 21.9 and 47.4% from days 2 to 6 (Figure 3K), which was in accordance with an increase of 21.5 and 48.5% for the NO concentration (Figure 3C). The untreated cells also showed a correlation between fluorescence intensity and NO levels. In the control groups, both L-NMMA and Andro stagnated the fluorescence intensity increased by IL-1 β . On day 6, the decrease was 11 and 23.9%, respectively (Figure 3J,L), which echoed the decline in the NO production (12.2% reduction by L-NMMA and 28.5% reduction by Andro; Figure 3E).

3.4. NO Nanosensors Fluorescence and NO Production Correlate with the Release of Proinflammatory/Procatabolic Mediators of IL-1 β -Stimulated Chondrocytes. NO is a pivotal inflammatory factor that contributes to the OA progression by the modulation of proinflammatory or procatabolic factors, including *Nos2*, *Il1b*, *Mmp13*, and *Ptgs2*.²² As shown in Figure 4, compared with the untreated cells, the gene expressions of *Nos2*, *Il1b*, *Mmp13*, and *Ptgs2* was upregulated in the IL-1 β -stimulated chondrocytes, which correlates with the increase in NO nanosensors fluorescence and NO secretion. In the treatment groups, both L-NMMA and Andro downregulated the expression of these proinflammatory/procatabolic factors, with the reduction correlating with the fluorescence and NO levels.

3.5. NO Accumulation Correlates with IL-1 β -Stimulated Collagen Type II and Aggrecan Degradation. Collagen type II and glycosaminoglycan (GAG) are cartilage-specific markers, which are related with cartilage degeneration. As shown in the RT-PCR results (Figure 4), the expression of the two genes *Col2a1* and aggrecan (*Acan*, a proteoglycan composed of GAGs) in the IL-1 β -stimulated chondrocytes declined when treated with IL-1 β . Both L-NMMA and Andro, and particularly Andro, inhibited the degradation of collagen

type II and GAG. The variation in both *Col2a1* and aggrecan correlated with the NO nanosensors fluorescence and NO levels.

3.6. NO Nanosensor for Tracking NO Secretion in Joints of OA Animals. As shown in Figure 5A, 0.5 h after injection was chosen as the optimal in vivo observation point. The fluorescence of knee joints and the NO production in joint fluid were detected in rats at weeks 4, 8, and 12 after ACLT operation, respectively. As shown in Figure 5B, the NO levels in the joint fluid increased with time, which is positively correlated with the increase in the NO nanosensor fluorescence. Correlation coefficient was as high as 0.880 (Figure 5C).

In agreement with the in vitro cell experiment, L-NMMA and Andro significantly reduced the NO production in the OA rats at week 8 (Figure 5D), which showed a positive correlation with the fluorescence decline. Correlation coefficient is 0.893 for the treatment group (Figure 5E). Importantly, almost no fluorescence could be detected at the joint when naked DAF-FM probes were injected (Figure 5F). Time-dependent in vivo fluorescence images further elucidate the prediction of OA progression as facilitated by the NO nanosensor (Figure 5G).

3.7. NO Nanosensors Fluorescence and NO Levels of the Joint Correlate with the Scores of OA. The changes in the articular cartilage in the OA development were examined using macroscopic observation, HE staining, and Safranin-O staining in the Supporting Information (Figure S2). The ACLT groups showed general characteristics of OA, including erosion, osteophyte formation, and large lesions of a severe grade and size (Figure 5H). Macroscopic scores on the cartilage lesions after ACLT operation were obviously higher than those in control; these scores also increased in a time-dependent manner. This indicates that the inflammation severity progressed with time. Histological grading on the structural changes, cellular changes, Safranin-O staining, and tide mark also confirmed the macroscopic observations. Both the clinical scores and the histopathological scores correlated well with the fluorescence intensity and the NO levels in the joint.

Meanwhile, both L-NMMA and Andro delivered through intra-articular injection significantly decreased ($p < 0.05$) the severity of the macroscopic lesions on the femoral condyles and tibial plateaus, which scored much lower than OA control in clinical and histological evaluations (Figure 5I). Accordingly, the fluorescence intensity of nanosensor weakened after the therapy, which reflected the clinical and histological scores well.

3.8. Correlation of Fluorescence and NO Levels with Cartilage Degeneration and OA-Related Biomarkers. Safranin-O staining and immunohistochemical analysis showed that collagen type II and aggrecan faded with time (Figure S2), indicating OA damage to cartilage-specific extracellular matrix. Administration of L-NMMA and Andro, and especially Andro, alleviated the degeneration of the cartilage matrix, as revealed through more intense staining for cartilage-specific markers. The trend for various cartilage-specific markers was negatively correlated with NO accumulation and fluorescence in the joint. In contrast, the expression of proinflammatory/procatabolic mediators including NOS2 and MMP13 increased with time (Figure 5J) and was downregulated by L-NMMA and Andro

treatment (Figure 5K). The expression of these OA-related markers was positively correlated with the fluorescence intensity and NO levels in the joint.

4. DISCUSSION

The OA chondrocytes overexpress iNOS and its product, NO,^{23,24} which has been considered as a biomarker for OA.²⁵ DAF-FM and its derivative DAF-FM diacetate are currently the most preferred sensors for the NO detection from plant tissues to living parasites.^{12,26} However, the small molecule DAF-FM quickly dilutes and dissipates once injected into the joint fluid, preventing its usage in the detection and tracking of the NO production in the joint (Figure 5F).

Nanoparticle-based sustained drug release has been widely studied in the past decades for targeted and sustained drug delivery.^{27,28} In this concept, nanoparticles act as both protector and reservoir for the drugs. In our study, the nanosensors were synthesized by encapsulating the DAF-FM within the biodegradable PLGA nanoparticles (Figure 2A). The size was controlled around 1000 nm to extend their cellular retention time (Figure 2B).²⁹ The surface of the nanosensors was modified with cationic polymer to facilitate cell internalization (Figure 2C). To confirm whether the nanoparticle encapsulation would achieve the preservation and protection of DAF-DM, the nanosensors were placed in a physiological buffer and the release profile of DAF-DM was derived by measuring the fluorescence of the supernatant (Figure 2D). There was 50% release of DAF-DM from the nanoparticles in the first 24 h, whereas the rest got out in the next 144 h (Figure 2D). As shown in Figure 2E, the stability of NO nanosensors versus DAF-FM probe was significantly extended to 20 days (480 h), which testified the protection of intact DAF-FM probe following nanoparticle encapsulation.

Next, we tested the NO nanosensors *in vitro* on chondrocytes. IL-1 β is known to inhibit the chondrocyte proliferation through the induction of NO secretion (Figure 3A,C). Besides, the secreted NO contributes to the OA progression by elevating the expression proinflammatory factors including *Nos2*, *Il1b*, *Mmp13*, and *Ptgs* and attenuating cartilage markers (*Col2a1* and *Acan*) (Figure 4). The presence of nitric oxide synthase inhibitors like L-NMMA and Andro could reduce the NO induction and the antiproliferative effect of IL-1 β in a time-dependent manner (Figure 3B,E). Accordingly, L-NMMA and Andro lowered the transcription responses of the IL-1 β -induced genes in the chondrocytes (Figure 4).

Subsequently, we labeled the chondrocytes with nanosensors and tracked their fluorescence for 6 days (Figure 3G–I,K). In this period, a gradual increase in the fluorescence was seen in both untreated and IL-1 β -treated cells, and the increase in the fluorescence intensity in both groups is consistent with the NO increase (Figure 3C). NO is produced in a normal tissue, but increases dramatically in abnormal conditions such as inflammation.¹⁰ The fluorescence can be detected in untreated cells, demonstrating the sensitivity of the NO sensor. However, the intensity is not high, which can hardly be detected *in vivo*. In the IL-1 β -treated cells, the fluorescence and NO production were much higher than that in the untreated cells, which agrees with previous reports that IL-1 β exposure to chondrocytes increases the NO release.^{30,31} The results indicated that NO sensor is applicable in pathological conditions, when NO is abnormally high. Treatment with L-NMMA or Andro would significantly reduce the fluorescence of cells from nanosensors

(Figure 3J,L). These results match very well with the change in NO concentrations in the chondrocytes (Figure 3E). It suggested that the proposed nanosensor could enter the cells and release DAF-DM in the cytoplasmic region. This DAF-DM then reacts with NO to produce the fluorescent signal. Although this platform improves the cell penetration of DAF-DM, it also extends the lifetime of DAF-DM in the cells from 6 to 144 h (i.e., 6 days) at least. Excited by the *in vitro* discoveries, we set off to explore the utilization of this nanosensor for the NO detection in the OA rat model. The OA model generated through ACLT presented the general characteristics of OA, including erosion, osteophyte formation, and large lesions with severe grade and size (Figure 5H). More importantly, the NO secretion was elevated in the joint fluid (Figure 5B). As observed in *in vivo* experiment, the expressions of *Nos2* and *Mmp13* were upregulated, whereas those of collagen type II and aggrecan were downregulated in the arthritic cartilage (Figure 5J). On the other side, both L-NMMA and Andro delivered through intra-articular injection had significantly decreased the OA severity with less NO secretion (Figure 5D,I).

Through intra-articular injection, the nanosensors were delivered to the joint 30 min before the imaging. In a period of 12 weeks, the fluorescence from nanosensors-labeled knees increased, which was associated with cartilage degeneration (Figure S2). Nanosensors signal also demonstrated the efficacy of drug therapy using L-NMMA and Andro for the treatment of OA. Comparatively, there was barely any fluorescence signal from the joint of OA animals when naked DAF-FM molecules were injected (Figure 5F). It is clear that free DAF-FM probes were swiftly diluted and dissipated in the joint fluid and tissues. This result confirms the importance of nanocarriers in protecting and storing molecular sensors.

5. CONCLUSIONS

In this study, we synthesize a NO nanosensor by encapsulating the NO-sensing molecules DAF-FM within the biodegradable PLGA nanoparticles to predict the OA progression. In our *in vitro* study, the novel synthesized nanosensor appears to smartly track the time-dependent NO release in the IL-1 β -stimulated chondrocytes and the alleviated effect of L-NMMA (a NO inhibitor) and Andro (an anti-inflammatory agent), as evidenced by the positive correlation of the fluorescence intensity with NO concentration and OA markers. In our *in vivo* study, the fluorescent probe smartly tracks NO level in the joint fluid *in vivo*, which was correlated with the severity of OA. The nanosensor also showed the longitudinal and stable tracking effect on the OA animals receiving therapy based on the intra-articular injection of L-NMMA and Andro. Overall, our results indicate that NO is a realistic molecular marker to predict OA progression, and the proposed NO nanosensors have the potential to be applied in the clinical diagnosis of OA severity and the evaluation of drug therapy.

ASSOCIATED CONTENT

S Supporting Information

The Supporting Information is available free of charge on the ACS Publications website at DOI: 10.1021/acsami.7b06404.

Cytotoxicity of Andro and L-NMMA (Figure S1) and macroscopic observation, histological examination, and immunohistochemical analysis of the OA-induced arthritis (Figure S2) (PDF)

AUTHOR INFORMATION

Corresponding Authors

*E-mail: zhengli224@163.com. Tel: +8607715358132. Fax:

+8607715350975 (L.Z.).

*E-mail: cixu@ntu.edu.sg. Tel: +656790 6086. Fax: +65 6791 1761 (C.X.).

ORCID

Pan Jin: 0000-0001-7218-9496

Chenjie Xu: 0000-0002-8278-3912

Author Contributions

#P.J., C.W., and J.Z. contributed equally.

Author Contributions

P.J., C.W., and J.Z. contributed equally. J.Z., L.Z., and C.X. conceived the idea; P.J., C.W. and J.Z. performed the research; P.J. and C.W. produced drafts of the manuscript with the advice from L.Z. and C.X. All of the authors approved the final version of the manuscript.

Funding

The work was sponsored by NTU-Northwestern Institute for Nanomedicine; LKC Medicine-SCBE Collaborative Grant; National key research and development program of China (2016YFB0700804); Guangxi Science Fund for Distinguished Young Scholars (Grant No. 2014GXNSFGA118006); Guangxi Scientific Research and Technological Development Foundation (Grant No. GuikeAB16450003); and High level innovation teams and outstanding scholars in Guangxi Universities (the third batch).

Notes

The authors declare no competing financial interest.

REFERENCES

- (1) Lawrence, R. C.; Felson, D. T.; Helmick, C. G.; Arnold, L. M.; Choi, H.; Deyo, R. A.; Gabriel, S.; Hirsch, R.; Hochberg, M. C.; Hunder, G. G.; Jordan, J. M.; Katz, J. N.; Kremers, H. M.; Wolfe, F. Estimates of the Prevalence of Arthritis and Other Rheumatic Conditions in the United States. Part II. *Arthritis Rheum.* **2008**, *58*, 26–35.
- (2) World Health Organization. *The Global Burden of Disease: 2004 Update*; WHO Press: Geneva, 2008.
- (3) Studer, R. K. Nitric Oxide Decreases IGF-1 Receptor Function in Vitro; Glutathione Depletion Enhances This Effect in Vivo. *Osteoarthritis Cartilage* **2004**, *12*, 863–869.
- (4) Nagy, G.; Clark, J. M.; Buzas, E.; Gorman, C.; Pasztoi, M.; Koncz, A.; Falus, A.; Cope, A. P. Nitric Oxide Production of T Lymphocytes is Increased in Rheumatoid Arthritis. *Immunol. Lett.* **2008**, *118*, 55–58.
- (5) Kheansaard, W.; Mas-Oo-di, S.; Nilganuwong, S.; Tanyong, D. I. Interferon-Gamma Induced Nitric Oxide-mediated Apoptosis of Anemia of Chronic Disease in Rheumatoid Arthritis. *Rheumatol. Int.* **2013**, *33*, 151–156.
- (6) Clancy, R. M.; Amin, A. R.; Abramson, S. B. The Role of Nitric Oxide in Inflammation and Immunity. *Arthritis Rheum.* **1998**, *41*, 1141–1151.
- (7) Karan, A.; Karan, M. A.; Vural, P.; Erten, N.; Tascioglu, C.; Aksoy, C.; Canbaz, M.; Oncel, A. Synovial Fluid Nitric Oxide Levels in Patients with Knee Osteoarthritis. *Clin. Rheumatol.* **2003**, *22*, 397–399.
- (8) Sato, S.; Wang, X.; Saito, J.; Fukuhara, A.; Uematsu, M.; Suzuki, Y.; Sato, Y.; Misa, K.; Nikaido, T.; Fukuhara, N.; Tanino, Y.; Munakata, M. Exhaled Nitric Oxide and Inducible Nitric Oxide Synthase Gene Polymorphism in Japanese Asthmatics. *Allergol. Int.* **2016**, *65*, 300–305.
- (9) Chan, J.; Dodani, S. C.; Chang, C. J. Reaction-Based Small-Molecule Fluorescent Probes for Chemoselective Bioimaging. *Nat. Chem.* **2012**, *4*, 973–984.
- (10) Kojima, H.; Nakatsubo, N.; Kikuchi, K.; Kawahara, S.; Kirino, Y.; Nagoshi, H.; Hirata, Y.; Nagano, T. Detection and Imaging of Nitric Oxide with Novel Fluorescent Indicators: Diaminofluoresceins. *Anal. Chem.* **1998**, *70*, 2446–2453.
- (11) Gupta, K. J.; Igamberdiev, A. U. Recommendations of Using at Least Two Different Methods for Measuring NO. *Front. Plant Sci.* **2013**, *4*, 58.
- (12) Vitecek, J.; Reinohl, V.; Jones, R. L. Measuring NO Production by Plant Tissues and Suspension Cultured Cells. *Mol. Plant* **2008**, *1*, 270–284.
- (13) Csonka, C.; Pali, T.; Bencsik, P.; Gorbe, A.; Ferdinand, P.; Csont, T. Measurement of NO in Biological Samples. *Br. J. Pharmacol.* **2015**, *172*, 1620–1632.
- (14) Wiraja, C.; Yeo, D. C.; Chong, M. S.; Xu, C. Nanosensors for Continuous and Noninvasive Monitoring of Mesenchymal Stem Cell Osteogenic Differentiation. *Small* **2016**, *12*, 1342–1350.
- (15) Fu, J.; Wiraja, C.; Chong, R.; Xu, C.; Wang, D. A. Real-Time and Non-Invasive Monitoring of Embryonic Stem Cell Survival During the Development of Embryoid Bodies with Smart Nanosensor. *Acta Biomater.* **2017**, *49*, 358–367.
- (16) Lu, Z.; Wu, H.; Lin, X.; Liu, B.; Lin, C.; Zheng, L.; Zhao, J. Chondro-Protective and Antiarthritic Effects of Sulfonamido-Based Gallate-ZXHA-TC in Vitro and in Vivo. *ACS Chem. Biol.* **2016**, *11*, 1613–1623.
- (17) Hayami, T.; Pickarski, M.; Zhuo, Y.; Wesolowski, G. A.; Rodan, G. A.; Duong, L. T. Characterization of Articular Cartilage and Subchondral Bone Changes in the Rat Anterior Cruciate Ligament Transection and Meniscectomized Models of Osteoarthritis. *Bone* **2006**, *38*, 234–243.
- (18) Pelletier, J. P.; DiBattista, J. A.; Raynauld, J. P.; Wilhelm, S.; Martel-Pelletier, J. The in Vivo Effects of Intraarticular Corticosteroid Injections on Cartilage Lesions, Stromelysin, Interleukin-1, and Oncogene Protein Synthesis in Experimental Osteoarthritis. *Lab. Invest.* **1995**, *72*, 578–586.
- (19) Mankin, H. J.; Dorfman, H.; Lippiello, L.; Zarins, A. Biochemical and Metabolic Abnormalities in Articular Cartilage from Osteoarthritic Human Hips. II. Correlation of Morphology with Biochemical and Metabolic Data. *J. Bone Jt. Surg., Am. Vol.* **1971**, *53*, 523–537.
- (20) Evans, J. D. *Straightforward Statistics for the Behavioral Sciences*; Brooks/Cole Publishing Co: Pacific Grove, CA, 1996.
- (21) Wang, Z.; Wang, M.; Carr, B. I. The Inhibitory Effect of Interleukin 1 Beta on Rat Hepatocyte DNA Synthesis is Mediated by Nitric Oxide. *Hepatology* **1998**, *28*, 430–435.
- (22) Abramson, S. B. Nitric Oxide in Inflammation and Pain Associated with Osteoarthritis. *Arthritis Res. Ther.* **2008**, *10*, S2.
- (23) Amin, A. R.; Di Cesare, P. E.; Vyas, P.; Attur, M.; Tzeng, E.; Billiar, T. R.; Stuchin, S. A.; Abramson, S. B. The Expression and Regulation of Nitric Oxide Synthase in Human Osteoarthritis-affected Chondrocytes: Evidence for Up-Regulated Neuronal Nitric Oxide Synthase. *J. Exp. Med.* **1995**, *182*, 2097–2102.
- (24) Melchiorri, C.; Meliconi, R.; Frizziero, L.; Silvestri, T.; Pulsatelli, L.; Mazzetti, I.; Borzi, R. M.; Uggioni, M.; Facchini, A. Enhanced and Coordinated in Vivo Expression of Inflammatory Cytokines and Nitric Oxide Synthase by Chondrocytes from Patients with Osteoarthritis. *Arthritis Rheum.* **1998**, *41*, 2165–2174.
- (25) Santoro, A.; Conde, J.; Scotece, M.; Abella, V.; Lopez, V.; Pino, J.; Gomez, R.; Gomez-Reino, J. J.; Gualillo, O. Choosing the Right Chondrocyte Cell Line: Focus on Nitric Oxide. *J. Orthop. Res.* **2015**, *33*, 1784–1788.
- (26) Kohn, A. B.; Lea, J. M.; Moroz, L. L.; Greenberg, R. M. SchistosomaMansonii: Use of AFUorescent Indicator to Detect Nitric Oxide and Related Species in Living Parasites. *Exp. Parasitol.* **2006**, *113*, 130–133.
- (27) El-Gogary, R. I.; Rubio, N.; Wang, J. T.; Al-Jamal, W. T.; Bourgognon, M.; Kafa, H.; Naem, M.; Klippstein, R.; Abbate, V.; Leroux, F.; Bals, S.; Van Tendeloo, G.; Kamel, A. O.; Awad, G. A.; Mortada, N. D.; Al-Jamal, K. T. Polyethylene Glycol Conjugated Polymeric Nanocapsules for Targeted Delivery of Quercetin to Folate-

Expressing Cancer Cells in Vitro and in Vivo. *ACS Nano* **2014**, *8*, 1384–1401.

(28) Yallapu, M. M.; Gupta, B. K.; Jaggi, M.; Chauhan, S. C. Fabrication of Curcumin Encapsulated PLGA Nanoparticles for Improved Therapeutic Effects in Metastatic Cancer Cells. *J. Colloid Interface Sci.* **2010**, *351*, 19–29.

(29) Xu, C.; Miranda-Nieves, D.; Ankrum, J. A.; Matthiesen, M. E.; Phillips, J. A.; Roes, I.; Wojtkiewicz, G. R.; Juneja, V.; Kultima, J. R.; Zhao, W.; Vemula, P. K.; Lin, C. P.; Nahrendorf, M.; Karp, J. M. Tracking Mesenchymal Stem Cells with Iron Oxide Nanoparticle Loaded Poly(lactide-co-glycolide) Microparticles. *Nano Lett.* **2012**, *12*, 4131–4139.

(30) Hayashi, T.; Abe, E.; Yamate, T.; Taguchi, Y.; Jasim, H. E. Nitric Oxide Production by Superficial and Deep Articular Chondrocytes. *Arthritis Rheum.* **1997**, *40*, 261–269.

(31) Zhou, P. H.; Liu, S. Q.; Peng, H. The Effect of Hyaluronic Acid on IL-1 Beta-Induced Chondrocyte Apoptosis in A Rat Model of Osteoarthritis. *J. Orthop. Res.* **2008**, *26*, 1643–1648.